Journal of Sulfur Chemistry
Publication details, including instructions for authors and subscription information:
http://www.informaworld.com/smpp/title~content=t713926081

Effect of cation vacancy and crystal superstructure on thermodynamics of iron monosulfides

Haipeng Wang[a]; Allan Pring[b]; Fei Wu[c]; Guorong Chen[d]; Jianhua Jiang[d]; Fang Xia[e]; Jian Zhang[d]; Yung Ngothai[e]; Brian O'neill[e]
[a] AJ Parker CRC for Hydrometallurgy, Bentley, WA, Australia [b] Department of Mineralogy, South Australian Museum, Adelaide, SA, Australia [c] School of Chemistry & Pharmacy, East China University of Science & Technology, Shanghai, P.R. China [d] School of Material Engineering, East China University of Science & Technology, Shanghai, P.R. China [e] School of Chemical Engineering, University of Adelaide, Adelaide, SA, Australia

To cite this Article Wang, Haipeng , Pring, Allan , Wu, Fei , Chen, Guorong , Jiang, Jianhua , Xia, Fang , Zhang, Jian , Ngothai, Yung and O'neill, Brian(2006) 'Effect of cation vacancy and crystal superstructure on thermodynamics of iron monosulfides', Journal of Sulfur Chemistry, 27: 3, 271 — 282
To link to this Article: DOI: 10.1080/17415990600646124
URL: http://dx.doi.org/10.1080/17415990600646124

Journal of Sulfur Chemistry
Vol. 27, No. 3, June 2006, 271–282

Taylor & Francis
Taylor & Francis Group

MINIREVIEW ARTICLE

Effect of cation vacancy and crystal superstructure on thermodynamics of iron monosulfides

HAIPENG WANG*†, ALLAN PRING‡, FEI WU§, GUORONG CHEN¶, JIANHUA JIANG¶, FANG XIA††, JIAN ZHANG¶, YUNG NGOTHAI†† and BRIAN O'NEILL††

†AJ Parker CRC for Hydrometallurgy, CSIRO Minerals, P.O. Box 90, Bentley, WA 6982, Australia
‡Department of Mineralogy, South Australian Museum, Adelaide, SA 5001, Australia
§School of Chemistry & Pharmacy, East China University of Science & Technology, Shanghai 200237, P.R. China
¶School of Material Engineering, East China University of Science & Technology, Shanghai 200237, P.R. China
††School of Chemical Engineering, University of Adelaide, Adelaide, SA 5005, Australia

(Received 13 December 2005; in final form 14 February 2006)

Iron monosulfides, $Fe_{1-x}S$ ($0 < x < 0.125$), are extremely complex in their chemical and physical behaviours, which are largely attributed to their nonstoichiometric nature and myriad superstructures. The chemical composition of $Fe_{1-x}S$ affects the polymorph formation for iron monosulfides, their mineral reactivity, surface sulfur fugacity, and thermal expansion. In this paper, the effects of cation vacancy and crystal superstructure on the thermodynamics of iron monosulfides are reviewed and discussed.

Keywords: Iron monosulfide; Vacancy; Nonstoichiometry; Pyrrhotite

1. Introduction

Iron monosulfides is also known as pyrrhotite group minerals that possess the NiAs-type substructure. [1, 2]. This term includes troilite, monoclinic and hexagonal pyrrhotites. They crystallize in the hexagonal or monoclinic system; troilite (FeS) is hexagonal, whereas pyrrhotite ($Fe_{1-x}S$) may be either monoclinic or hexagonal. These minerals appear usually in massive form, and occur chiefly in basic igneous rocks. Interest in the pyrrhotite group arises from their occurrence in metallurgical process, their properties, and their common occurrence in ore deposits of many types. They are all derivatives of the NiAs structure [3, 4]. Pyrrhotite minerals are abundant in nature, dark, brownish rusty colour on the surface, commonly found in ultrabasic rocks, hydrothermal mineral deposits, and contact-metasomatiic sediments. They

*Corresponding author. Email: haipeng.wang@adelaide.edu.au

Journal of Sulfur Chemistry
ISSN 1741-5993 print/ISSN 1741-6000 online
http://www.tandf.co.uk/journals
DOI: 10.1080/17415990600646124

are often in paragenesis with pyrite, chalcopyrite, pentlandite, and magnetite. Better understanding of the effects of cation vacancy and crystal superstructure on the thermodynamics of iron monosulfides is of commercial interest for mineral processing industry. For the clarity of discussion, the results being presented were thermodynamic data of synthetic materials.

2. Polymorphs

2.1 *Troilite*

Troilite is a stoichiometric or near stoichiometric iron sulfide ($Fe_{1-x}S$, $x = 0 \sim 0.05$), having 2C superstructure of NiAs-type ($a = \sqrt{3}A$, $c = 2C$ where A and C are the axes of the NiAs subcell common to troilite and pyrrhotites), and $P\bar{6}2c$ symmetry below 140 °C [5–10]. It has a hexagonal close packed structure with [FeS_6] and [SFe_6] units. Troilite shows distortions from ideal NiAs lattice positions (figure 1a); triangular groupings of iron atoms are displaced in the ab-plane forming contracted and dilated triangular units. The sulfur network is much less distorted with only a slight displacement of one-third of the sulfur atoms along the c axis, away from the centre of Fe cluster [11]. The Fe cluster formed by three Fe atoms on ab-plane is shown in figure 1b. Neighboring Fe triangular clusters are positioned in two ways: stack directly above one another along c axis, and situated obliquely above one another (figure 1). Thus, a line connecting Fe atoms along c axis is alternately parallel and inclined to c. The position of a iron cluster in the troilite cell is shown in figure 1c. The formation of Fe-Fe cluster is caused by Fe-Fe bonds formed by 3d electron overlapping when Fe-Fe distances below the critical value, 3.0 Å [12].

In nature, troilite is not as abundant as other metal deficient pyrrhotite ores, and forms under strong reducing conditions [7]. One such reducing environment is in swamps, where anaerobic bacteria can reduce sulfate to sulfide. Studies of swamp sediments show only low concentrations of troilite, but an abundance of fine crystalline pyrite [11].

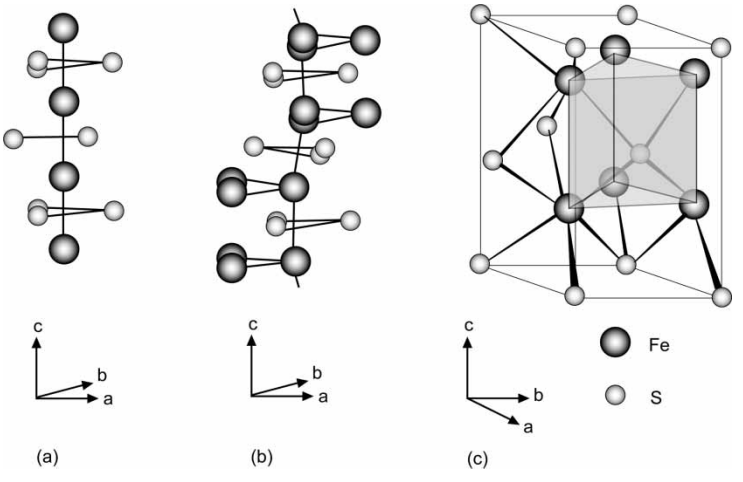

Figure 1. (a) Partial configuration of S and Fe atoms long c axis in the NiAs structure. (b) Partial atom configuration in troilite along c axis. Triangular Fe clusters are surrounded by distorted sulfur octahedrons. (c) Fe clusters in the troilite cell, which is derived from the NiAs cell by doubling the c axis, with a axis deviating by 30° in ab-plane [12, 53].

2.2 *Monoclinic pyrrhotite*

Monoclinic pyrrhotite can be perceived as a derivative from FeS by substraction of one iron atom per eight (FeS) units. The resultant structure contains layers of Fe sites separated from layers of iron sites with vacancies by sulfur atoms, thereby lowering the symmetry of the system from hexagonal (FeS) to monoclinic (Fe_7S_8) [13, 14]. The 4C monoclinic structure may be regarded as the result of a slight distortion of the hexagonal structure [15], in which the c axis tilts with respect to the basal ab-plane [16]. The phase Fe_7S_8 adopts a monoclinic structure in which vacancies are confined to every other site in alternate rows of sites within the vacancy layer. The vacancy layers are stacked in an ABCD sequence, quadrupling the unit cell along the stacking direction and leading to a superstructure of 4C. The various vacancy arrangements, A D, are shown in figure 2a.

The 4C (quartet along c axis) superstructure of pyrrhotite can be expressed as (. . . FAFBFCFDF. . .), where F represents a layer free of cation vacancies (figure 2b). Monoclinic pyrrhotite is not stable at high temperatures. Synthetic pyrrhotites through quenching technique are normally hexagonal even if the bulk composition were prepared with iron and sulfur in proportions appropriate to Fe_7S_8. Subsequent prolonged annealing at around 200°C is required to convert hexagonal Fe_7S_8 to monoclinic Fe_7S_8 [17].

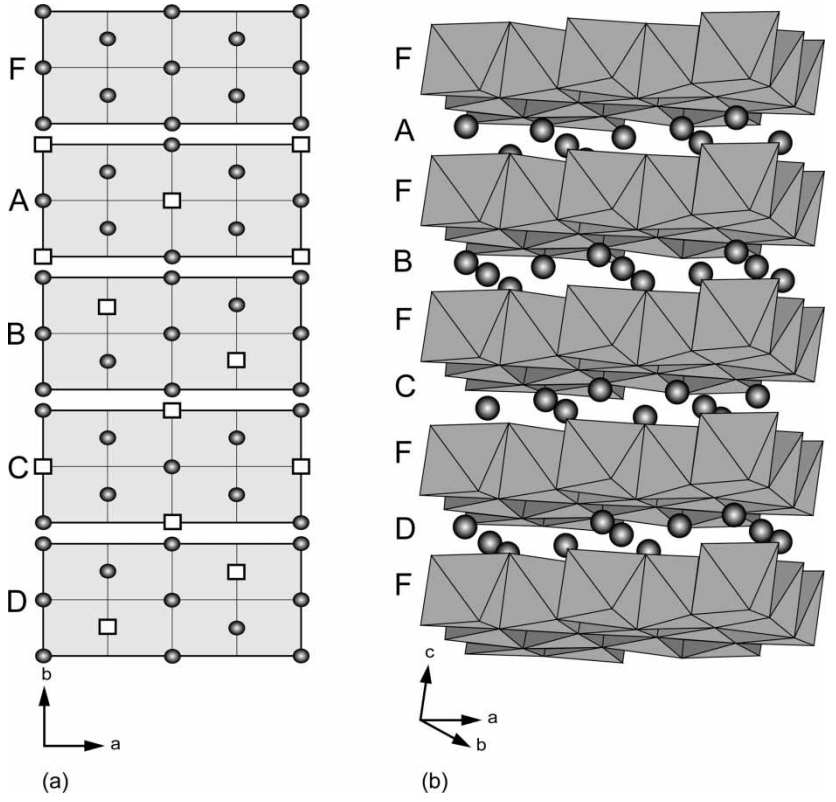

Figure 2. 4C monoclinic superstructure of pyrrhotite. (a) four different vacancy arrangements in cation layer, A, B, C, and D. (b) Stacking sequence of vacancy layers and vacancy free layers [13, 14].

2.3 *Hexagonal pyrrhotites*

Same as in monoclinic pyrrhotite, vacancy layers in hexagonal pyrrhotites determine the structural and magnetic properties of the various phases in pyrrhotite group (from monoclinic to hexagonal NC structures). The phase relations between different superstructures are shown in figure 3. A repulsion effect among vacancies in pyrrhotite was observed. This observation was further developed by Powell (1983) into the *Vacancy Avoidance* theory, which has been used to study the superstructures of pyrrhotite caused by vacancy ordering [18]. At high temperatures, the vacancy distribution is random and the unit cell of pyrrhotite is equivalent to the NiAs subcell, as called 1C structure [19]. When the temperature decreases, the vacancies start to order and form superstructures of NiAs subcell [20]. At very low temperatures (<300 °C), the diffusion of vacancies is extremely inhibited that the preservation of high-temperature structure becomes possible [21–24]. Many natural hexagonal pyrrhotites were formed during

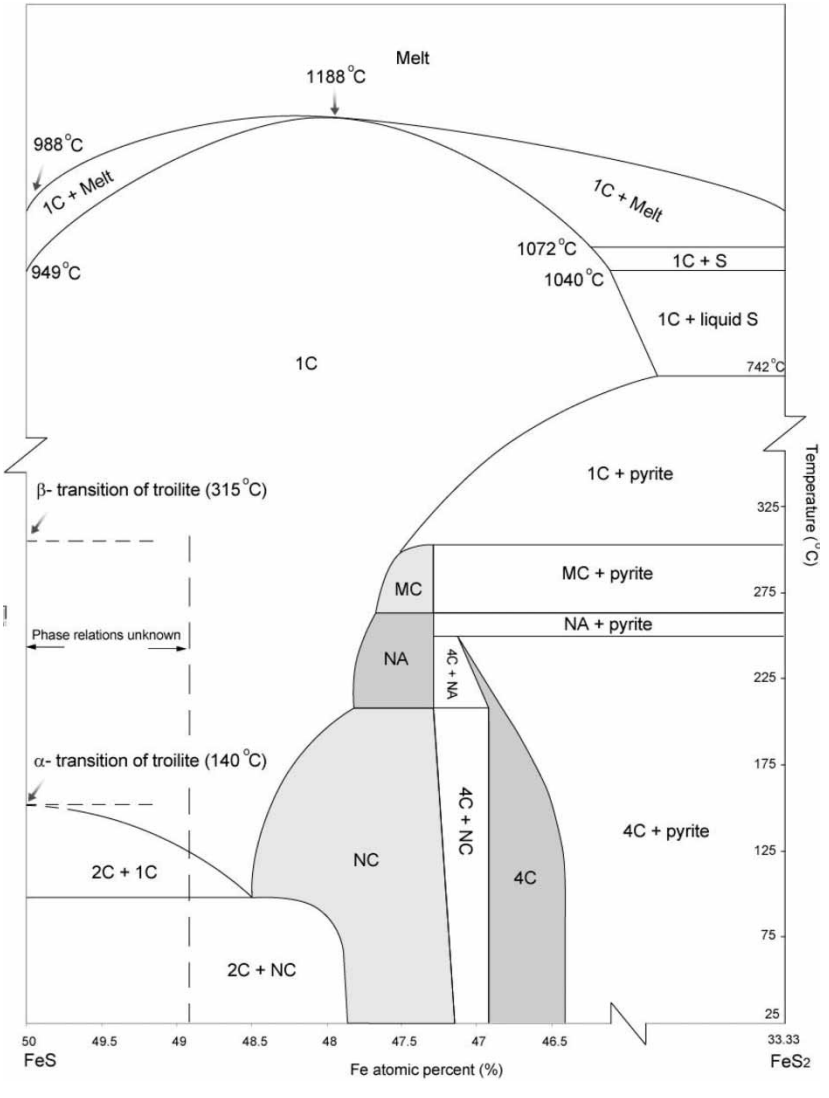

Figure 3. FeS-FeS_2 phase diagram [5, 30, 43, 58, 61, 63].

a quenching process. The superstructures of NiAs subcell, except for 4C and 2C (see figure 3), contain nonintegral x-ray reflections attributed to the statistical contribution to diffraction maxima determined by domain structures involving filled and partially filled iron sublattices [25]. Formation of superstructures does not affect the short-range atom configurations. Many of these hexagonal superstructures have very close composition but they appear to behave as separate phases and were normally treated as such when delineating phase diagrams. The hexagonal structures of MC (2A/MC, $M = 3.0 \sim 4.0$), NA (NA/3C, N varies continuously between 40 and 90), and NC-types (2A/NC, N varies continuously between 3.0 and 6.0 [26]) were described by Nakazawa and Morimoto (1970, 1971) [27, 28]. The trigonal structure of pyrrhotite is considered a special case of hexagonal pyrrhotite when $M \approx 3$. The most commonly found superstructures in nature, 5C (Fe_9S_{10}), 6C ($Fe_{11}S_{12}$), and 11C ($Fe_{10}S_{11}$), characterized by their c-axis periodicity, can all be related to one or more of Nakazawa and Morimoto's classifications [26, 29]. These superstructures are also described in terms of stacking of fully occupied and ordered defective iron layers normal to the c-axis. Each structure is characterized by a regular succession of such layers, corresponding to an integral supercell multiplicity N, where $c = NC$ (C is the c parameter of NiAs subcell). The multiplicity N is related to the general chemical formula $Fe_{m-1}S_m$ ($m > 8$) by $N = 0.5\,m$ (when m has a even value), or $N = m$ (when m has an odd value) [29]. This formulism only serves for the convenience of describing the superstructures in pyrrhotite. In fact, pyrrhotites with nonintegral multiplicity superstructure are more common, as the m (as in $Fe_{m-1}S_m$) is not necessary integer and changes continuously with composition and temperature [29]. Deviations from the ordered succession give rise to non-integral N values, and thus to an incommensurate c-axis [30–32]. These pyrrhotites are often referred to as hexagonal pyrrhotite, which have compositions in the region of at.% Fe between troilite and monoclinic pyrrhotite. These superstructures can either expressed as Fe_9S_{10}, $Fe_{10}S_{11}$, $Fe_{11}S_{12}$ or a mixture of the stoichiometric phases with troilite or with monoclinic pyrrhotite [13, 26, 33, 34].

3. Enthalpy, entropy, and Gibbs free energy

When reactions involve pyrrhotite group minerals, it is practical to use thermodynamic parameters (G, S, H) to evaluate the nature of a reaction such as: equilibrium conditions, and activation energies of a reaction. These parameters vary with temperature, pressure, activity, etc., but they all can be deduced from the values of these parameters under standard conditions (1 atm., activity of pure chemical = 1). A large number of experimental studies and evaluation of the equilibrium thermodynamic properties of pyrrhotite group are available [35–41]. Their results are comparable. The standard molar enthalpies and entropies of pyrrhotite formation have been systematically measured for non-stoichiometric compositions ($Fe_{1-x}S$, $0 < x < 0.125$) using calorimeter [30]. The standard molar Gibbs free energy of formation of these non-stoichiometric compounds can be deduced in a statistical model proposed by Sølen and Grønvold (1987) [39]. In order to compare the thermodynamic properties of different pyrrhotite compositions, the molar thermodynamic parameters are normalized to per mole atoms rather than per molecular formula (e.g. FeS and $Fe_{0.98}S$ are normalized to (1/2)FeS and (1/1.98)$Fe_{0.98}S$, respectively). The enthalpy and entropy of formation for pyrrhotite group within composition range FeS to $Fe_{0.858}S$ are illustrated in figures 4a and b.

These properties vary with composition and temperature, therefore only curves for the boundary compositions FeS to $Fe_{0.858}S$ are shown in figure 4 for clearer representation. The standard molar Gibbs free energy of formation ($\Delta_f G^o_m$) is most useful in determination

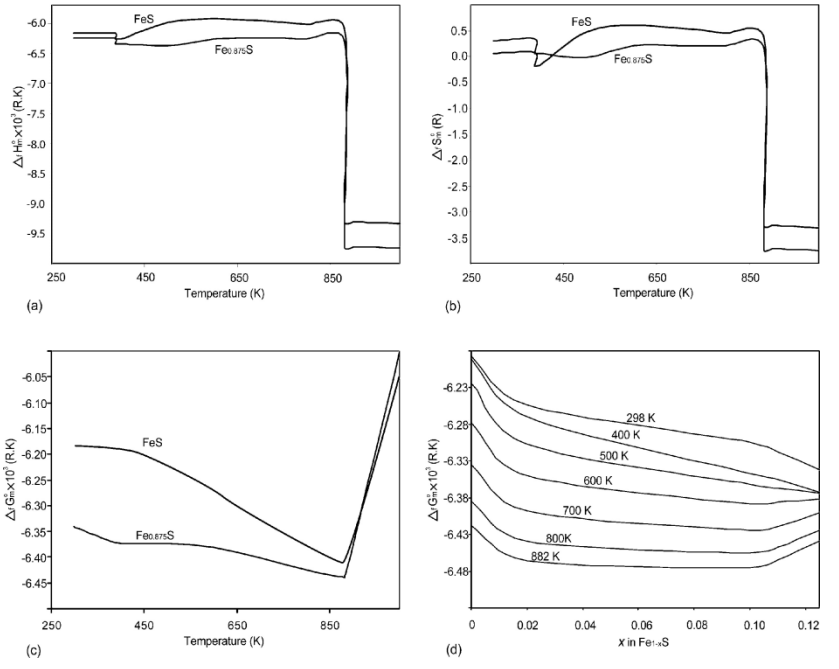

Figure 4. Variation of (a) standard molar formation enthalpy, (b) standard molar formation entropy, and (c) standard molar formation Geeb's free energy of pyrrhotite with temperature. (d) Variation of standard Geeb's free energy with x (as in $Fe_{1-x}S$) [30].

of the direction and tendency of a reaction. Figures 4c and d show the $\Delta_f G^o_m$ dependence on pyrrhotite composition and temperature.

4. Dependence of sulfur fugacity on stoichiometry

There are many published data on the dependence of sulfur fugacity on the non-stoichiometry of pyrrhotite [18, 38, 42]. The equilibrium between S in pyrrhotite and S vapor can be written as:

$$S_{po} \longleftrightarrow \frac{1}{2}S_2 \uparrow \tag{1}$$

where S_{po} is the sulfur in pyrrhotite; S_2, the sulfur vapor.

The chemical potential of sulfur in both states follows the equation:

$$\mu_{S,po} = \frac{1}{2}\mu_{S_2\uparrow} \tag{2}$$

where $\mu_{S,po}$ and $\mu_{S_2\uparrow}$ are chemical potential of sulfur in pyrrhotite and sulfur vapor respectively.

The equilibrium sulfur fugacity of non-stoichiometric pyrrhotite $Fe_{1-x}S$ depends on both x and temperature. The upper limit of x is 0.125, the Fe_7S_8 composition. The defects in pyrrhotite are mainly Fe vacancies, which are depicted by x. The interactions between Fe atoms and the vacancies are likely to be very strong, vacancies preferring Fe rather than vacancy nearest

neighbors. Therefore, the chemical potentials in equilibrium are related as:

$$\mu_{S,po} = \mu_{\lambda S} = \mu^{\circ}_{\lambda S} + RTlnx + (2\varepsilon_{Fe\lambda} - \varepsilon_{FeFe} - \varepsilon_{\lambda\lambda})(1-x)^2 \quad (3)$$

where $\varepsilon_{Fe\lambda}$ and ε_{FeFe}, and $\varepsilon_{\lambda\lambda}$ are paring energy between Fe-vacancy, Fe-Fe, and vacancy-vacancy, respectively. R is gas constant. T is temperature. Thus, the Darken's quadratic formalism is derived by substituting equation (2) to (3). It provides the justification for plotting sulfur fugacity data against x. The formula is shown as follows [43]:

$$\ln f_{S2} = \frac{2}{RT}[A + B(1-x)^2] + \ln x \quad (4)$$

where f_{S2} is the sulfur fugacity in equilibrium. $A = \mu^{\circ}_{\lambda S}$ -μ_{S2} ↑. $B = 2\varepsilon_{Fe\lambda} - \varepsilon_{FeFe} - \varepsilon_{\lambda\lambda}$ Rau (1976) and Powell (1983) have studied extensively on the relation between f_{S2} and x and concluded that within the x range $0 < x < 0.125$ the B is a constant of -206 kJ [18, 41]. The parameter A can be determined as a function of temperature using the least square method fitting the data of Rau (1976) as: $A/kJ = 0.09T/K + 68$ [41]. Therefore, the empirical equation of $\ln f_{S2}$ vs x is:

$$\ln f_{S2} = \frac{2}{RT}[0.09T - 206(1-x)^2 + 68] + \ln x \quad (5)$$

As shown in equation (5), sulfur fugacity is a function of pyrrhotite composition and temperature. Extra care should be taken when using equation (5) to relate f_{S2}, T, and x, as this equation was deduced on the assumption that no new phase exsolved in the temperature range. In another word, this equation only valid for a two phases system, sulfur gas-homogeneous pyrrhotite.

5. Dependence of FeS activity on stoichiometry

It has been proven that point defects in pyrrhotite are mainly iron vacancies [18, 41, 44–48]. The vacancies on iron sites can be expressed as a solid solution between the stoichiometric FeS and λS, a fictive solid with pyrrhotite structure but all the cation sites are empty. The activities for stoichiometric FeS and pure λS under standard state are defined as 1. Pyrrhotite group $Fe_{1-x}S$ has activity state that deviates from its stoichiometric composition, therefore its activity ($\alpha_{FeS} \neq 1$). The solid solution is described as:

$$(1-x)FeS + xS \longrightarrow Fe_{1-x}S \quad (6)$$

In this nonideal solid solution, the activity coefficient (γ) is related to the mole fraction (N) as follows:

$$RTln\gamma = G^{\infty}_{ex}(1-N)^2 \quad (7)$$

Where G^{∞}_{ex} is the excess partial molar free energy at infinite dilution [41, 45].

Activity (α) is related to the activity coefficient and mole fraction by $\alpha = \gamma N$. Then, gives:

$$RTln\alpha_{FeS} = RTlnN_{FeS} + G^{\infty}_{ex}(1-N_{FeS})^2 \quad (8)$$

where $N_{FeS} = 1 - x$ according to equation (6). The Dependence of FeS activity on x, then, can be written as:

$$RTln\alpha_{FeS} = RTln(1-x) + G^{\infty}_{ex}x^2 \quad (9)$$

The value of G^{∞}_{ex} has been experimentally determined by Froese (2003) and Rau (1970) to be $-218.18\,kJ.mol^{-1}$ [41, 45].

6. Thermal Expansion

The thermal expansivity of solid-state minerals is well represented by the following equation:

$$\gamma(T) = \Delta l / l_0 \tag{10}$$

where $\Delta l = l_T - l_0$, l_T and l_0 are linear length of sample at arbitrary temperature T and room temperature 25 °C, respectively [51, 52].

Due to the overlapping of adjacent Fe outmost t_{2g} orbitals parallel to c-axis, the Fe-Fe distance along c-axis is shorter than that in ab-plane [53]. Thus, pyrrhotite is more rigid //c than ⊥c, indicating possible anisotropic thermal expansivity. This was proved by Tsatis (1988) who measured the $\gamma \sim \gamma\ (T)$ curve of monoclinic pyrrhotite (Fe_7S_8) (figure 5) [51].

The thermal expansivity is positive in the temperature range 25 to 300 °C for the basal ab-plane. In the direction //c, however, the thermal expansion curve shows a projectile nature, becoming negative after T > 120 °C.

The anisotropism of pyrrhotite thermal expansivity determines different thermal expansive behavior along different crystal axis. It may arise from the anisotropic internal stress field [52]. The resulting anisotropic thermal expansion is in good agreement with the fact that the average Fe-Fe distance along c-axis in pyrrhotite is smaller than that in ab-plane [54]. It is convenient to integrate these direction dependent variables into one parameter, which includes all the contributions from these variables. Thus, this parameter does not vary with direction. It is more convenient to be used to describe the physical property of pyrrhotite. A widely used

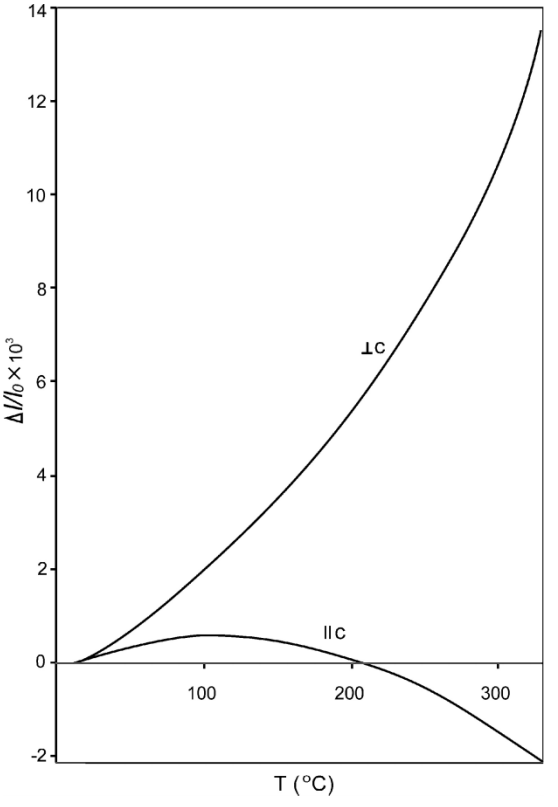

Figure 5. The fractional change in length of pyrrhotite crystal perpendicular and parallel to c axis as a function of temperature [51, 52].

parameter of this kind is thermal expansion coefficient (α), is generally defined by:

$$\alpha = \frac{1}{V_0} \cdot \frac{dV}{dT} \tag{11}$$

where V_0 is the cell volume at a reference temperature (usually the lowest temperature in the considered thermal range). dV/dt is the change rate in cell volume with temperature.

Taylor (1970) and Tenailleaul (2005) investigated the thermal expansivity of a series of pyrrhotite sample with various compositions. The results showed that the pyrrhotite composition does not significantly affect its thermal expansivity a slight decrease in thermal expansivity occurs when pyrrhotite samples become more metal deficient, indicating that the thermal expansion is damped by vacancy ordering or clustering [55, 56].

With increasing temperature pyrrhotite undergoes a magnetic transition at 315°C (β-transition), transforming from ferrimagnetic to paramagnetic structure, accompanied by abrupt cell parameter variations [57]. Wang and Salveson [63] explained the mechanism of the magnetic structural transition in details. Tenailleaul *et al.* [56] stated that pyrrhotite will undergo a significant increase in thermal expansivity when $T < T_\beta$ (β-transition temperature, 315 °C). It has been reported that the mean thermal expansion coefficients in the temperature range 315 ∼ 500 °C ($T > T_\beta$) for pyrrhotite compositions FeS, $Fe_{0.84}Ni_{0.11}S$ are 7.4 and $8.0 \times 10^{-5}\,K^{-1}$, respectively. These values increase to $14.1 \times 10^{-5}\,K^{-1}$ (FeS) and $9.3 \times 10^{-5}\,K^{-1}$ ($Fe_{0.84}Ni_{0.11}S$) for temperature range 100 ∼ 315 °C ($T < T_\beta$) [56].

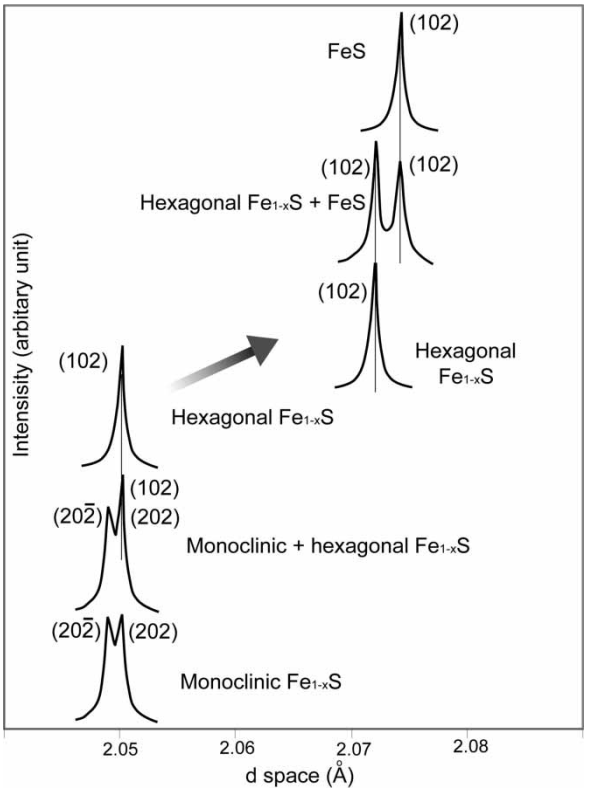

Figure 6. d_{102} Reflection position of NiAs subcell for different pyrrhotite phases [61].

7. Dependence of d_{102} reflection on superstructures

X-ray diffraction pattern has been successfully used for phase identification within pyrrhotite group. The crystal structure of pyrrhotite group minerals can be more or less described as superstructures of NiAs-type. The differences among the x-ray diffraction patterns for these minerals, sometimes, are almost imperceptible due to poor crystallinity. However, the diffraction peak of (102) plane (a subcell plane of NiAs-type) is quite sensitive to composition and superstructure type. Generally peaking, the d-space of (102) peak decreases in the sequence of monoclinic pyrrhotite < hexagonal pyrrhotite < troilite. The decreasing d-space is related to the increase in iron vacancy from FeS to Fe_7S_8 (shown in figure 6).

The shape and location of the d space of (102) in an x-ray diffraction pattern are commonly used to qualitatively identify different pyrrhotite phases (e.g. monoclinic, hexagonal pyrrhotite, and troilite). A single sharp peak (located at the right end in figure 6) having the largest d_{102} is from for FeS (troilite). The clearly separated double peaks, second pattern to the right end in figure 6, represents FeS + hexagonal phases. The d_{102} of hexagonal pyrrhotite varies in a wide range (from the third peak from left to the fourth one from left) due to its wide composition range [58–60]. When pyrrhotite structure becomes monoclinic the former (102) peak splits into two reflections (202) and $(20\bar{2})$ (pattern at the left end in figure 6) [61, 62]. These two peaks of monoclinic pyrrhotite ((202) and $(20\bar{2})$) have approximately equal intensity and 0.006 Å apart [62]. The second pattern from left is a split reflection with the intensity of the higher angle $(20\bar{2})$ reflection less than the other reflection (202) + (102), indicating a mixture of hexagonal pyrrhotite and monoclinic pyrrhotite.

8. Dependence of d_{102} reflection on composition

The composition vs d_{102} relation of Yund and Hall (1969) is widely used to quantitatively determine the pyrrhotite compositions [63]. d_{102} in x-ray diffraction pattern varies with the composition of pyrrhotite. The empirical is:

$$Y = 45.212 + 72.86(d_{102} - 2.0400) + 311.5(d_{102} - 2.0400)^2 \tag{12}$$

Where Y is the composition of hexagonal pyrrhotite in atomic percent iron. The standard error for this relation is 0.06 atomic percent iron.

As this method only applies to hexagonal pyrrhotites, the bulk compositions of monoclinic pyrrhotite or mixtures of monoclinic+hexagonal pyrrhotites should be determined by converting the monoclinic pyrrhotite to a metastable hexagonal pyrrhotite through a heating process. An example is shown as follows for the compositional determination for each phase in a mixture consists of monoclinic (M) + hexagonal (H) pyrrhotites.

Step 1 H is calculated to have composition Fe_hS; composition of M unknown; Weight percentage of H equals to p.

Step 2 Heat the mixture (M + H) to temperature > 610°C, then quench in cold water. The monoclinic pyrrhotite (M) has been converted to hexagonal pyrrhotite (H). Charge shows a homogenous hexagonal structure.

Step 3 Bulk composition of the quenched charge is calculated to be Fe_XS.

Step 4 The former monoclinic pyrrhotite (M) has composition Fe_mS. m can be expressed as:

$$m = \frac{XhN_{Fe}(1-p) + N_S(X-hp)}{N_{Fe}(h-X) + N_S(1-p)} \tag{13}$$

where m, h, and X correspond to the iron contents shown as in Fe_mS, Fe_hS, and Fe_XS. N_{Fe} and N_S are the mole weights for Fe and S. p is the weight percentage of the original hexagonal pyrrhotite in the charge.

9. Concluding remarks

Iron monosulfide minerals are abundant in nature, involved in myriad mineralogical and metallurgical fields. However, they are extremely complicated from both a crystallographic and chemical standpoint due to their nonstoichiometric nature, various polymorphs, and variable magnetic and electronic properties a better understanding of the mineral chemistry and physics of these minerals benefits many industrial and scientific areas. There are many compositional and crystallographic variations of pyrrhotite minerals merit considerations from researchers with different backgrounds.

Acknowledgements

We thank Australian Research Council and CSIRO Minerals for their financial support.

References

[1] R.G. Arnold. *Am. Mineral.*, **51**, 1221 (1966).
[2] R.H. Carpenter, G.A. Desborough. *Am. Mineral.*, **49**, 1350 (1964).
[3] H.W. Nesbitt, A.G. Schaufuss, G.M. Bancroft, R. Szargan. *Phys. Chem. Minerals* **29**, 72 (2002).
[4] D.J. Vaughan, J.R. Craig. *Mineral Chemistry of Metal Sulphides*, Cambridge University Press, Cambridge (1978).
[5] S.A. Kissin, S.D. Scott. *Econ. Geol.*, **77**, 1739 (1982).
[6] E.F. Bertaut. *Comptes Rendus*, **234**, 1295 (1952).
[7] H.T. Evans. *Science* **167**, 621 (1970).
[8] F. Li, H.F. Franzen. *J. Alloys and Compd.*, **238**, 73 (1996).
[9] J.C. Ward. *Rev. Pure and Appl. Chem.*, **20**, 175 (1970).
[10] J.M.D. Coey, H. Roux-Buisson, R. Brusetti. *J. Phys.*, **C4**, 1 (1976).
[11] J.E. Thomas, W.M. Skinner, R. St.C. Smart. *Geochim. Cosmochimi. Acta*, **67**, 831 (2003).
[12] O. Kruse. *Am. Mineral.*, **75**, 755 (1990).
[13] J.W.A. Kondoro. *J. Alloys Compd.*, **289**, 36 (1999).
[14] L.M. Levinson, D. Treves. *J. Phys. Chem. Solids.*, 29, 2227 (1968).
[15] J. Flahaut. *Transition metal chalcogenides: International Review of Science, Solid State Chemistry, Inorganic Chemistry.* Butterworths University Park Press, London (1972).
[16] M. Corlett. *Zeitschrift fur Kristallographie*, **126**, 124 (1968).
[17] W. O'Reilly, V. Hoffmann, A.C. Chouker, H.C. Soffel, A. Menyeh. *Geophys. J. Int.*, **142**, 669 (2000).
[18] R. Powell. *Mineral. Mag.*, **47**, 437 (1983).
[19] N. Morimoto. *Memoirs Inst. Sci. Ind. Res. Osaka Uni.*, **36**, 45 (1978).
[20] H. Nakazawa, N. Morimoto. *Am. Mineral.*, **60**, 359 (1975).
[21] L.A. Marusak, L.L. Tongson. *J. Appl. Phys.*, **50**, 4350 (1979).
[22] K. Igaki, M. Sata. *Trans. Jpn. Inst. Met.*, **22**, 627(1981).
[23] K. Igaki, M. Sata, T. Shinohara. *Trans. Jpn. Inst. Met.*, **23**, 221 (1982).
[24] K. Ono, A. Ito, E. Hirahara. *J. Phys. Soc. Jpn*, **17**, 1615 (1962).
[25] L. Pierce, P.R. Buseck. *Science*, **186**, 1209 (1974).
[26] N. Morimoto, A. Gyobu, K. Tsukuma, K. Koto. *Econ. Geol.*, **70**, 824 (1975).
[27] H. Nakazawa, N. Morimot. *Jpn. Acad. Proc.*, **46**, 678 (1970).
[28] H. Nakazawa, N. Morimoto. *Mat. Res. Bull.*, **6**, 345 (1971).
[29] N. Morimoto, A. Gyobu, K. Tsukuma, K. Koto. *Am. Mineral.*, **60**, 240 (1975).
[30] F. Grønvold, S. Stølen. *J. Chem. Thermodynamics*, **24**, 913 (1992).

[31] K. Koto, N. Morimoto, A. Gyobu. *Acta Cryst.*, **B31**, 2759 (1975).
[32] N. Morimoto. *Rec. Prog. Nat. Sci. Jpn.*, **3**, 183 (1978).
[33] L.F. Power, H.A. Fine. *Miner. Sci. Eng.*, **8**, 107 (1976).
[34] N.S. Ovanesyan, G. Trukhtanov, Y.G. Odinets, G.V. Novikov. *Sov. Phys. J. Exp. Theor. Phys.*, **33**, 1193 (1971).
[35] L. Cemic, O. Kleppa. *J. Phys. Chem. Minerals*, **16**, 172 (1988).
[36] J.L. Haas, M. Chase. *Open File Report 89*. US Geological Survey. (1989).
[37] M.W. Chase, C.A.Davies, J.R. Downey, D.J. Frurip, R.A. McDonald, A.N. Syverud. *J. Phys. Chem. Ref. Data Suppl. "JANAF Thermochemical Tables, 3rd ed."*, **14**, 1 (1985).
[38] P. Toulmin, P.B. Barton. *Geochim. Cosmochim. Acta*, **28**, 641 (1964).
[39] S. Stølen, F.Grønvold. *J. Phys. Chem. Solids*, **48**, 1213 (1987).
[40] F. Grøvold, E.F. Westrum, C. Chou. *J. Chem. Phys.*, **30**, 528 (1959).
[41] H. Rau. *J. Phys. Chem. Solids*, **37**, 425 (1976).
[42] W. Burgmann, G. Urbain, M.G. Frohberg. *Mem. Sci. Rev. Metallurg.*, **65**, 567 (1968).
[43] L.S. Darken. *Trans. Met. Soc. A.I.M.E.*, **80**, 239 (1967).
[44] G. Hägg, I. Sucksdorff. *Zeit. Physik. Chem.*, **B22**, 444 (1933).
[45] E. Froese. *Can. Mineral.*, **41**, 1061 (2003).
[46] G.G. Libowitz. *J. Solid State Chem.* **1**, 50 (1969).
[47] G.G. Libowitz. *Energetic of defect formation and interaction in nonstoichiometric pyrrhotite. In Reactivity of Solids*, Chapman and Hall Press, London (1972)
[48] G.G. Libowitz J.B. Lightsone. *J. Phys. Chem. Solids*, **28**, 1145 (1967).
[49] E. Froese. *Geol. Surv. Can. Pap.*, **43,** 75 (1976).
[50] E. Froese. *Geol. Surv. Can. Pap.*, **80,** 28 (1981).
[51] D.E. Tsatis. *J. Phys. Chem. Solids*, **49**, 359 (1988).
[52] D.E. Tsatis. *J. Phys. Chem. Solids*, **48**, 489 (1987).
[53] W.M. Skinner, H.W. Nesbitt, A.R. Pratt. *Geochim. Cosmochim. Acta*, **68**, 2259 (2004).
[54] S. Sakkopoulos, E. Vitoratos, T. Argyreas. *J. Phys. Chem. Solids*, **45**, 923 (1984).
[55] L.A. Taylor. *Carnegie Inst. Washington Year Book.*, **68**, 259 (1970).
[56] C. Tenailleaul, B. Etchmann, H. Wang, A. Pring, B.A. Grguric, A. Studer. *Mineral. Mag.*, **69**, 205 (2005).
[57] A.V. Powell, P. Vaqueiro, K.S. Knight, L.C. Chapon, R.D. Sánchez. *Phys.Rev. B* **70**, 014415–1 (2004).
[58] R.G. Arnold. *Econ. Geol.*, **57**, 72 (1962).
[59] R.G. Arnold, L.E. Reichen. *Am. Mineral.*, **47**, 105 (1962).
[60] A.R. Graham. *Am. Mineral.*, **34**, 462 (1949).
[61] A. Byström. *Arkiv. For Kemi. Min. Geol.* B **19**, 1 (1945).
[62] R.A. Yund, H.T. Hall. *Econ.Geol.*, **64**, 420 (1969).
[63] H. Wang, I. Salveson. Phase Transitions **78**, 547 (2005).